Non-planar curvature and branching of arteries and non-planar-type flow

By Colin G. Caro[1], Denis J. Doorly[1], Maria Tarnawski[1], Katherine T. Scott[1], Quan Long[1] and Charles L. Dumoulin[2]

[1]*Centre for Biological and Medical Systems, Imperial College of Science, Technology and Medicine, Sir Leon Bagrit Centre, Exhibition Road, London SW7 2BX, UK*

[2]*GE Corporate Research and Development Center, PO Box 8, Schenectady, NY 12301, USA*

In this study, magnetic resonance imaging techniques have been used to examine the geometry of arterial curvature and branching in casts and *in vivo*, and to measure the distribution of axial velocity in the associated flow. It is found, contrary to a widely held view, that the geometry is commonly non-planar. Moreover, relatively small values of the parameters which render the geometry non-planar appear significantly to affect the velocity distribution. The findings suggest that non-planarity is an important factor influencing arterial flows, including wall shear. The implications are not restricted to vascular biology, pathology and surgery, but may extend to the design of general piping systems.

1. Introduction

The geometry of arteries influences their blood flow pattern and hence their biology and susceptibility to disease (Kamiya & Togawa 1980; Frangos *et al.* 1985; Schettler *et al.* 1983; Henderson 1991). It is evident that arteries branch and are often curved. It is also found that there is variation of the geometry between individuals (Friedman *et al.* 1983) and that it is affected by skeletal and other physiological motion (Caro *et al.* 1992; Pao *et al.* 1992). The loci generated by tracing the cross-sectional centre of an artery and any branches in the flow direction may be used to establish the geometry of the curvature and branching. It is planar if the space curves corresponding to the loci lie in a plane; otherwise it is non-planar.

At any point on a space curve, the local tangent vector and a vector along the radius of curvature define a plane; torsion measures the rate at which the orientation of this plane varies along the curve. Curvature and torsion are thus required to describe a non-planar curve, such as a helix, whereas only curvature is required to describe a planar curve. Pao *et al.* (1992) have used both parameters to quantify the time-dependent geometry of the canine coronary arteries. Branching complicates the geometric description, because it allows for discontinuities in the parameters where curves join. For example, at a branch or bifurcation, the curves corresponding to the joining arterial segments may each be planar, but with respect to differently oriented planes. Here the value of torsion is zero, apart from at the join point, where it has a δ-function behaviour, and the non-planarity arises from the discontinuity in orientation of the planes. (Although the primary emphasis in this work is on the geometrical

Proc. R. Soc. Lond. A (1996) **452**, 185–197
Printed in Great Britain

arrangement of the flow conduits, it is recognized that initial and boundary conditions (inlet velocity profile, shape and diameter of artery cross-section) also affect the flow.)

Most studies of flow in arterial bends and branches assume planar geometry (Schettler 1983; Yoshida *et al.* 1988; Liepsch 1990, 1994; Mosora *et al.* 1990). In studies which consider non-planar arterial geometry, attention is mainly focused on specific locations: aortic arch (Caro *et al.* 1971; Farthing & Peronneau 1979; Paulsen & Hasenkam 1983; Frazin *et al.* 1990; Yearwood & Chandran 1984; Kilner *et al.* 1993; Hoydu *et al.* 1994); branching of superficial coronary arteries (Batten & Nerem 1982; Altobelli & Nerem 1985; Sabbah *et al.* 1984); bifurcation of aorta (Moore *et al.* 1994); branching of femoral artery (Back *et al.* 1985); distal femoral artery (Scholten & Wensing 1995); and carotid syphon (Perktold *et al.* 1988). These studies reveal (or model) local flow patterns that are different from those expected with planar geometry (Dennis & Ng 1982; Berger *et al.* 1983; Lou & Yang 1992).

It is recognized that the geometry of natural blood vessels is far more complicated than that of model vessels and that the local flow pattern depends on the local geometry and the velocity distribution in the incoming flow (Sabbah *et al.* 1984; Asakura & Karino 1990; Karino *et al.* 1994). However, it does not appear to have been proposed previously that non-planarity is commonly required to describe the curvature and branching of the arteries and the associated flow. A crude model study, where introduction of a bend upstream of, and non-planar to, an existing bend was found to produce a swirling type of flow and to improve clearance of material from the flow system, provided motivation for the present work.

In the work, the geometry of the human aorta and the rabbit aorta at sites of curvature and branching is examined using casts. In addition, non-invasive magnetic resonance imaging (MRI) techniques are used to measure the geometry and flow pattern in arteries in a small group of healthy human subjects, and in a simple model.

2. Measurement of non-planar arterial geometry and flow

The cast of the human aorta and the rabbit aorta were prepared according to the method of Tompsett (1967). The studies of the geometry and flow pattern in the arteries in healthy human subjects were performed by MRI using a 1.5 T scanner (GE Medical Systems, Milwaukee, WI). Imaging sequence parameters are given. The subjects were aged 20–32 years and the studies were undertaken with Ethical Committee approval.

(*a*) *Studies in casts*

The human aortic cast was made of 'Woods metal' alloy and silicone rubber moulds were made of the arch and abdominal segment. The moulds were filled with dilute copper sulphate solution and images were acquired using a 3D gradient echo sequence (TR 33 ms, TE 9 ms, flip angle 10°) to obtain contiguous 1 mm slices through the mould with an in-plane resolution of 0.6 mm. The slices were processed using the AVS package (Advanced Visual Systems Inc.) to produce 3D data sets which could be displayed as rotated 2D projections to demonstrate the non-planar nature of the aortic arch and abdominal aorta.

The curvature of the aortic arch was approximately helical. The slices through the aortic arch and abdominal aorta showed curvature of the origins of the major

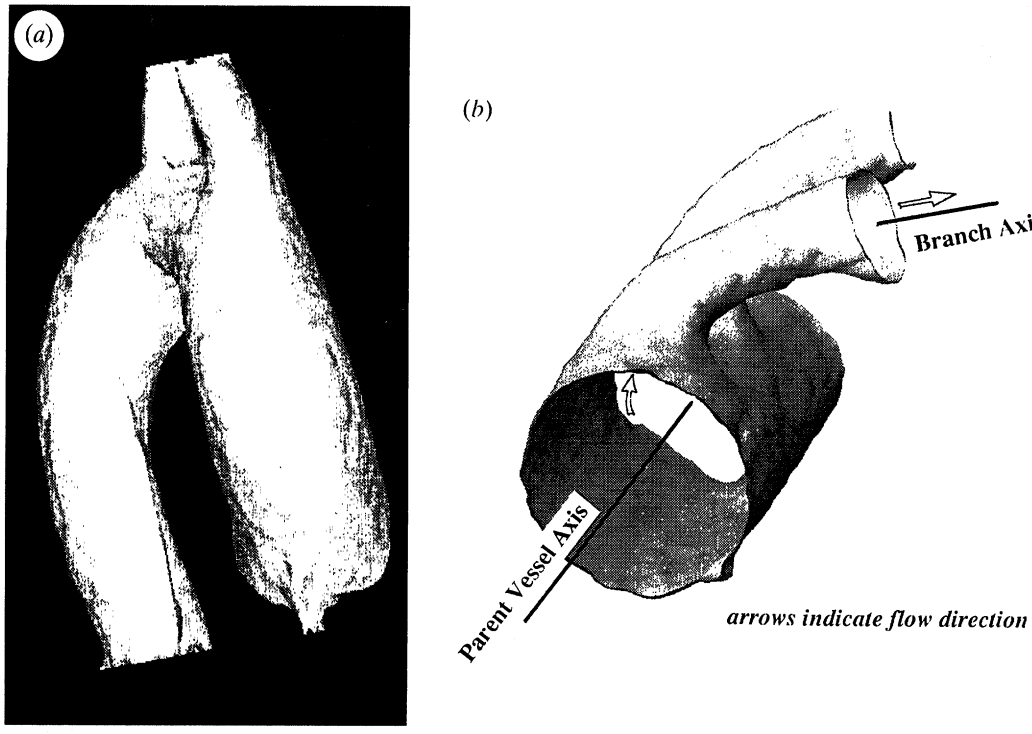

Figure 1. Reconstructed views of cast of human aorta. (*a*) A projected view of the aortic arch; the arch has helical-type curvature and there is curvature of the origins of the branches. (There is a streaking artefact over the descending aorta, caused by the reconstruction technique). (*b*) The origins of the branches of the abdominal aorta: the branching geometry can be expected to force the flow to follow a path with helical-type curvature, indicated by the arrows.

branches (figures 1*a*, *b*). The aortic bifurcation in the human cast was essentially planar, unlike *in vivo* (Moore *et al.* 1994; Caro *et al.* 1994*a*, *b*; Doorly *et al.* 1994). The rabbit cast showed approximately helical curvature of the aortic arch. In addition, there was curvature of the orgins of major branches of the aortic arch and abdominal aorta, and non-planarity of the trifurcation.

(*b*) *In vivo studies*

(i) *Aortic bifurcation*

MR angiographic images were obtained at the aortic bifurcation in six subjects, using a thick-slice 2D phase contrast gradient echo sequence (TR 33 ms, TE 9 ms, flip angle 20°) gated to the subject's ECG in order to reduce pulsatile blood flow artefacts. The images are 2D projections through a 28 cm thick section of tissue in coronal and sagittal planes, having an in-plane resolution of 1.25 mm. All images were encoded for a maximum velocity of 100 cm s^{-1}.

Velocity images were obtained at the aortic bifurcation in the six subjects who were studied angiographically, using a 2D cine phase contrast sequence (TR 30 ms, TE 12.6 ms, flip angle 30°, maximum velocity 80 cm s^{-1}). The 1 cm excitation slab was located 2 cm downstream of the aortic bifurcation and rotated about two independent axes, so as to be normal to the axis of one common iliac artery rather than to projections of the axis.

The angiographic studies revealed the aortic bifurcation to be non-planar in all

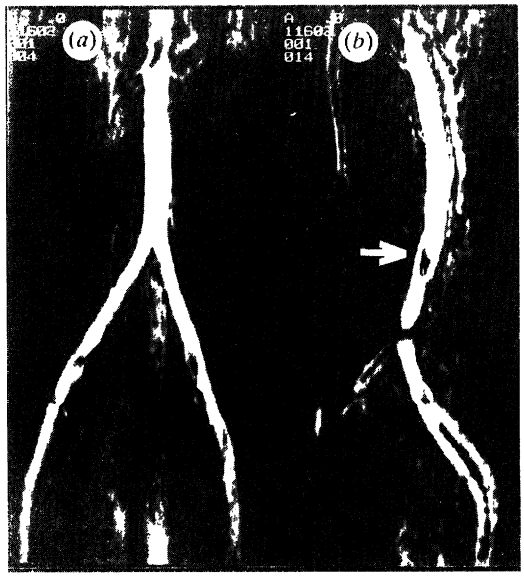

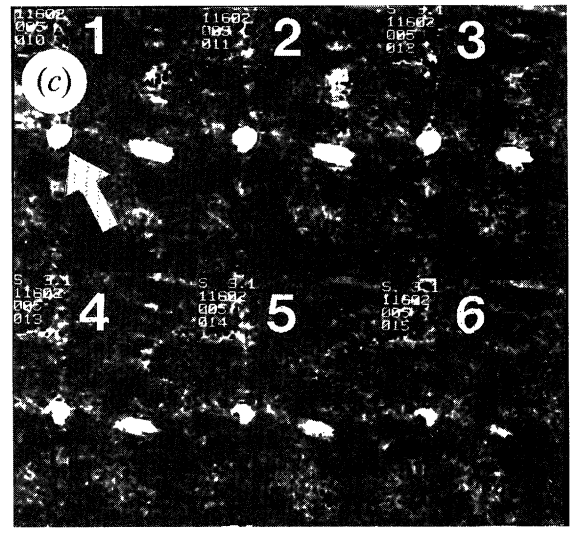

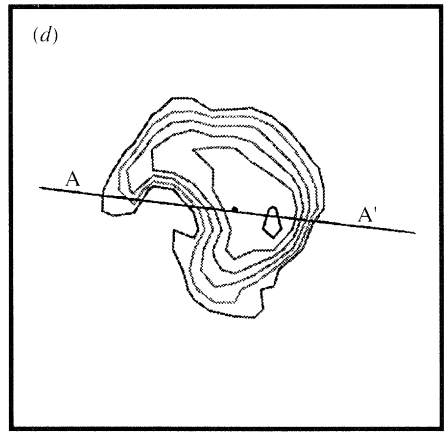

Figure 2. Shown are (*a*) coronal and (*b*) sagittal MRI views of the aortic bifurcation of a healthy human subject (arrow indicates level of bifurcation). (*c*) and (*d*) show the distribution of axial velocity in the right common iliac artery of the same subject (arrowed). The six phase images (1–6) in (*c*) were acquired at approximately 30 ms intervals, starting 250 ms after the ECG R-wave. Shown in (*d*) is the axial velocity contour plot from phase image 4. The velocity distribution is rotated out of the 'plane' of bifurcation (line A–A′) and is asymmetric.

the subjects. In the sagittal projection plane, the abdominal aorta and the bifurcation (figures 2*a*, *b*) show curvature (convexity anterior). Thus, the curve along the centreline of the abdominal artery, which branches into the two daughter (common iliac) arteries, possesses torsion at the bifurcation. Although the curvature measured in the sagittal projection was mild (radius of curvature typically 20 × aortic radius) flow effects were found. There was variation of the axial velocity distribution during the cardiac cycle (figure 2*c*) with the development of secondary motion. The secondary motion caused a crescentic distribution of axial velocity but, unlike in a planar bifurcation, the crescents were asymmetric and rotated out of the 'plane' of bifurcation (figure 2*d*). Measured looking upstream, the angle of rotation was about 70° anti-clockwise for the right common iliac artery and 75° clockwise for the left.

(ii) *Carotid artery bifurcation*

MR angiograms of the carotid artery bifurcation were obtained in four subjects, using a 2D time-of-flight gradient echo sequence (TR 47 ms, TE 8.7 ms, flip angle 45°) with venous saturation to acquire 64 contiguous 1.5 mm slices with an in-plane resolution of 0.8 mm. The images were processed using AVS (as described above) to obtain both coronal and sagittal views of the bifurcation.

Axial velocity images were obtained, using the 2D cine phase contrast sequence (TR 33 ms, TE 7.5 ms, flip angle 45°) 1 cm downstream of the carotid bifurcation in two of the four subjects studied angiographically. The measurements were encoded for a maximum velocity of 60 cm s^{-1} with a resolution of 0.5 mm.

The bifurcation appeared non-planar in all the subjects; both the left and right common carotid arteries ran laterally as well as axially towards the bifurcation, whereas at their origins the daughter vessels (internal and external carotid arteries) ran relatively axially (figure 3*a*, *b*). Figure 3*c* shows velocities measured 1 cm downstream of the left common carotid bifurcation in one subject. The axial velocity distribution in the carotid sinus was asymmetric and rotated out of the 'plane' of bifurcation during part of the cardiac cycle. The angle of rotation was about 45° clockwise, measured looking upstream. As noted, both features are consistent with non-planar geometry. Others have observed curvature of the terminal common carotid artery and helical-type flow in carotid bifurcation models (Masawa *et al.* 1994).

(iii) *Vertebral artery coalescence*

Coronal and sagittal views of the basilar and vertebral arteries were obtained in three subjects using a 3D phase contrast gradient echo sequence (TR 24 ms, TE 8.7 ms, flip angle 20°, maximum velocity 50 cm s^{-1}) to acquire 60 contiguous 1.5 mm slices with an in-plane resolution of 0.9 mm. Reconstruction of these views is carried out automatically on the GE Signa MR system. In all the subjects, the coalescence of the vertebral arteries to form the basilar artery appeared to be non-planar (figure 4*a*, *b*).

(*c*) *Model flow study*

We constructed a phantom to provide non-planar geometry and flow relevant to the arterial system. It was made of 15 mm id glass tubing and comprised two successive planar bends (75° arc, radii/radii of curvature about 0.1) arranged approximately orthogonally; the cross section of the tubes at the two bends was slightly elliptical (major/minor axis approximately 1.2, minor axis in plane of curvature) (figure 5*a*). The flow was steady and laminar (Reynolds number 850) and was fully developed at the entrance to the first bend. In order to image the flow, the phantom was placed in a standard quadrature head coil. The working fluid was a dilute solution of copper sulphate in distilled water. Two flexible tubes of different diameter were positioned 90° apart along the length of the phantom. They were filled with dilute copper sulphate and served as indicators of its orientation.

Thick slice localizing 2D phase contrast angiograms were obtained (TR 33 ms, TE 9 ms, flip angle 20°, 256 × 128, FOV 32 cm, Venc 15 cm s^{-1}, GRASS, scan time 1.5 min). In addition, thin slice oblique 2D phase contrast angiograms were obtained to localize a plane perpendicular to the tube axis (TR 33 ms, TE 10 ms, flip angle 30°, GRASS, slice thickness 20 mm, 256 × 128, NEX 20, scan time 1.5 min). Velocity measurements were made with a 3D phase contrast sequence, using a fast gradient

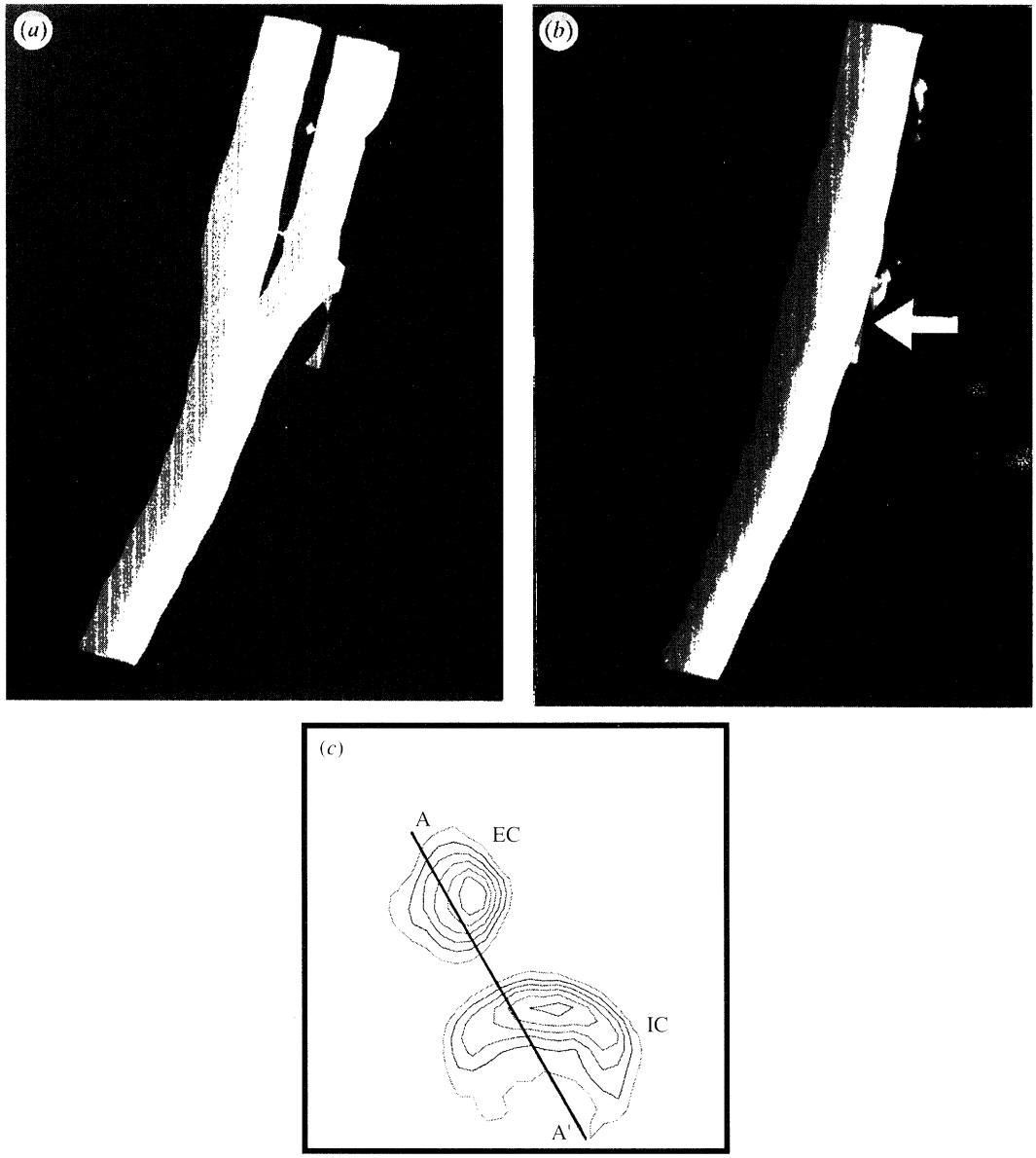

Figure 3. Reconstructed views showing (*a*) coronal and (*b*) sagittal MRI projections of the bifurcation of the left common carotid artery of a healthy human subject. Arrows denote the location of bifurcation. The sagittal projection shows curvature in the 'plane' of bifurcation, which renders the bifurcation non-planar. (Artefacts are seen, caused by the reconstruction technique.) Shown in (*c*) are axial velocity contour plots for internal (IC) and external (EC) carotid arteries, acquired 1 cm downstream of the bifurcation. The axial velocity distribution is seen to be rotated out of the 'plane' of bifurcation (A–A′) and to be asymmetric.

echo sequence with two spatial dimensions and a third dimension converted to a velocity dimension by the inclusion of a bipolar gradient. Each image showed the same spatial position, but a specific velocity range, that is image velocity contours in the axial (z) direction (TR 44.1 ms, TE 31.6 ms, flip angle 30°, FOV 10 cm, 256×128.

Figure 4. MR angiograms of the intracranial vessels of a healthy human subject. The coronal view (*a*) shows the coalescence of the vertebral arteries to form the basilar artery. The sagittal view (*b*) shows curvature in the 'plane' of coalescence, which renders the coalescence non-planar. Arrows denote the location of coalescence.

0.4 mm resolution, slice thickness 3 mm, velocity sensitivity 1 cm s^{-1}, 32 images: 1–16 representing -16 cm s^{-1} to -1 cm s^{-1}; 17–32 representing $+1$ to $+16$ cm s^{-1}, NEX 4, scan time 12 min).

At the first bend (figure 5*b*), the distribution of axial velocity was skewed symmetrically about the plane of curvature, with a substantially steeper near-wall velocity gradient at the outer wall than inner wall of curvature. At the second bend (figure 5*c*), the distribution of axial velocity was slightly asymmetric and rotated out of the plane of curvature. There were roughly 'diametrically' opposed regions of high and low near-wall velocity gradient, but the near-wall velocity gradient was substantially more uniform 'circumferentially' than at the first bend.

3. Discussion

We consider first the methods. Although the aortic casts were prepared *in situ* and at physiological transmural pressure, there could have been distortion *post-mortem*. Such distortion could explain why in the cast the human aortic bifurcation was essentially planar, whereas *in vivo* it was non-planar. It should be added that the *in vivo* studies involved only a small number of subjects.

In the MR measurement techniques, there is averaging within voxels, which will give rise to problems of spatial resolution. However, the resolution was adequate to determine the overall geometry of the vessels and hence to assess non-planarity. The use of 1 cm slices limits the accuracy of measurement of velocity, because of intravoxel averaging of velocities. Nevertheless, the images showed the rotation and asymmetry of the velocity distribution expected with flow in non-planar geometries (Batten & Nerem 1982; Kao 1987). Therefore, intravoxel velocity dephasing would not seem to have significantly limited velocity measurement. The velocity contours shown in the figures are unscaled, but could be scaled given additional information or the use of additional imaging sequences (Dumoulin *et al.* 1993). The 2D cine phase contrast

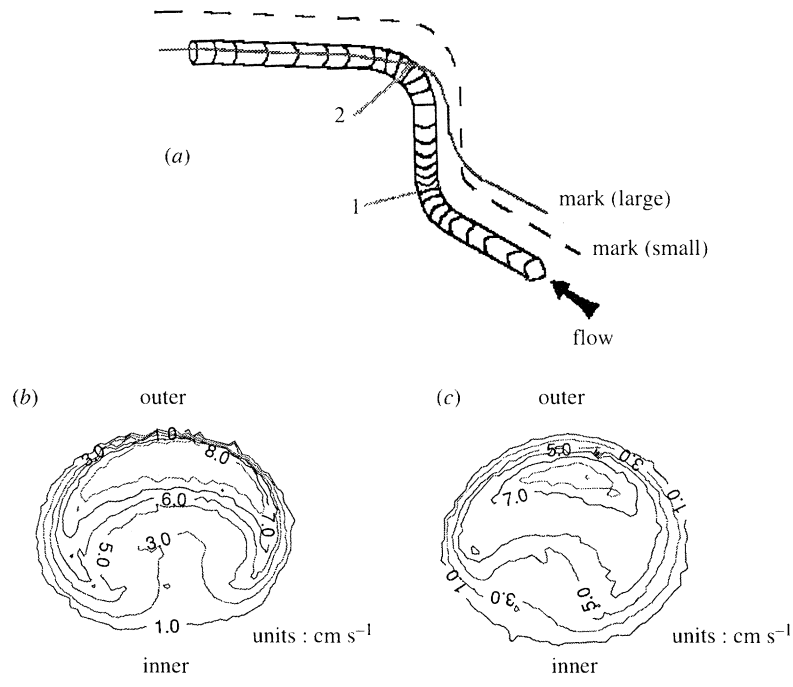

Figure 5. (*a*) the non-planar curved phantom, the location of the marker tubes along it, and the positions of the two stations used for MR velocity measurements. (*b*) shows the axial velocity distribution at station 1 (planar bend). The velocity distribution is symmetrical about the plane of curvature, with a substantially steeper near-wall velocity gradient at the outer than inner wall of curvature. (*c*) shows the axial velocity distribution at station 2 (second bend). The axial velocity distribution is slightly asymmetric and rotated out of the plane of curvature, and the near-wall velocity gradient is substantially more uniform 'circumferentially' than at the first bend.

sequence used acquires data continuously during the cardiac cycle and the data are retrospectively reconstructed to create the images. Some time averaging will therefore occur. However, previous experience with the technique, combined with experience gained from the use of more accurate but lengthier imaging sequences in phantoms, suggests that this would not have seriously limited the measurements.

The present studies confirm findings by others, that the curvature of the aortic arch and, usually, the bifurcation of the aorta are non-planar. In addition, they show that the bifurcation of the carotid arteries and the coalescence of the vertebral arteries to form the basilar artery are non-planar. Moreover, they suggest that the origins of major branches from the aortic arch and the abdominal aorta are non-planar; it has not yet been possible to measure the flow at these sites, or at the vertebral-basilar coalescence. It has been recognized previously that the geometry is non-planar at the branching of superficial coronary arteries and the femoral artery, and of the curvature of the distal femoral artery and carotid syphon. Therefore, the curvature and branching of the larger arteries appears commonly to be non-planar. Furthermore, the non-planarity appears to be locally helical.

The studies also show that the flow pattern just downstream of the aortic and carotid bifurcations differs from the symmetrical counter-rotational two (or more) vortex pattern found with planar geometry (Dennis & Ng 1982: Berger *et al.* 1983: Lou & Yang 1992) (see § 4). Instead, it resembles the flow pattern seen at the branch-

ing of coronary arteries and the bifurcation of the aorta (Batten & Nerem 1982; Moore *et al.* 1994), computed for the carotid artery syphon (Perktold *et al.* 1988) and that seen in the non-planar phantom. Non-planar curvature and branching of arteries thus appears to be associated with a distinctive flow pattern.

Flow in helical pipes is widely used in engineering applications, but has been little studied theoretically (Manlapaz & Churchill 1980: Wang 1981; Germano 1982; Kao 1987). The secondary motion in fully developed flow in a helical pipe, like that in a planar bend, consists of a pair of vortices. However, it can be much distorted, with one vortex being squeezed into a narrow region (Kao 1987). The asymmetry of the distribution of axial velocity, which was observed in the present work downstream of both the aortic and carotid bifurcations and in the non-planar phantom, is similar to that found by Kao (1987) for steady flow in a helical tube with sufficiently large torsion (see § 4).

The flow was mainly measured within and just downstream of non-planar regions, but the need to measure the flow upstream, in the transition region and further downstream, is recognized. Relevant studies by others include those of Yearwood & Chandran (1984), Frazin *et al.* (1990). Kilner *et al.* (1993), Hoydu *et al.* (1994), Moore *et al.* (1994), Sabbah *et al.* (1984). Masawa *et al.* (1994) and Scholten & Wensing (1995). In some of these studies, swirling or helical-type flow is reported downstream of a non-planar region, but it is important to distinguish between the symmetrical counter-rotational vortex pattern seen at planar bends and branches and the asymmetric distribution of axial velocity observed with non-planar geometry.

Earlier research, including that reviewed by Berger *et al.* (1983), has highlighted the role of entrance effects in flow in simple curved tubes. Clearly this work should be extended to flow in non-planar geometries, particularly since the interval between successive branches is often relatively short in the larger arteries. It would also be of interest to compare the flow through a non-planar feature, such as a bifurcation, where the entrance velocity distribution is axisymmetric, with that through a similar but planar bifurcation with asymmetric entrance velocity distribution. The small secondary velocity components have not been directly measured in the work reported here, because of difficulty in accurately positioning the measuring plane and accurately measuring them.

It can be expected that there will be greater mixing and a circumferentially more uniform wall shear with non-planar than planar geometry. Indicator dispersion studies, which we have undertaken, gave results consistent with these expectations (Johnson *et al.* 1994). Furthermore, in the present phantom study, the near-wall velocity gradient was circumferentially more uniform with non-planar than planar geometry.

In the light of current understanding, it can be anticipated that the flow patterns observed *in vivo* will influence the development and distribution of arterial disease, including atherosclerosis (Schettler *et al.* 1983: Yoshida *et al.* 1988; Liepsch 1990, 1994). Fox *et al.* (1982), Masawa *et al.* (1994) and Scholten & Wensing (1995) have reported a helical distribution of atherosclerotic lesions downstream of non-planar regions, consistent with a helical distribution of low wall shear.

Spiral flow patterns found at angioscopy during vascular reconstruction in infrainguinal arteries have been attributed to endoluminal spiral folds or 'rifling' (Stonebridge & Brophy 1991). However, the foregoing and the absence of folds or 'rifling' from normal arteries suggests an alternative explanation—that the flow patterns result from non-planar geometry and the folds or 'rifling' in diseased arteries represent helical distributions of lesions. Spiral flow has been demonstrated with biplanar

Doppler ultrasound in the common femoral arteries (Stonebridge *et al.* 1994). Its rotation in opposite directions in the right and left legs has been considered to imply a secondary flow phenomenon as a result of the aortic bifurcation. These flow patterns may have implications for other arterial pathology and vascular surgery (Stonebridge *et al.* 1991; Caro *et al.* 1994*b*): in graft-related intimal hyperplasia, the disease process appears to affect preferentially regions which experience low wall shear (Dobrin *et al.* 1989; White *et al.* 1993; Ojha 1994).

The apparently common occurrence of non-planar curvature and branching, and of non-planar-type flow in the larger arteries, poses several questions. One of these concerns the mechanisms which underlie non-planarity: it is likely that anatomical factors are involved, but it is also possible that fluid mechanical factors, including wall shear, play a role. A related question concerns the biological significance of non-planar-type flow. The thrust of the present work is to stimulate further study of the interaction between fluid mechanics and vascular biology. It appears that non-planarity is commonly found in the large vessels (although a complete characterization of the geometries and their distribution has yet to be performed). In the microcirculation, where the fluid mechanical regime is different, both two- and three-dimensional arrays of vessels are seen (Secomb *et al.* 1995).

Several fluid mechanical questions arise from the study, which merit investigation. Whilst the work has examined the non-planar geometry of arteries at a number of locations and has shown apparently strong sensitivity of flow to non-planarity, as yet the conditions upstream and downstream, at higher Reynolds numbers, and with unsteady flow have not been examined. It may be expected that the design of arteries is optimized, within certain limits, for the role of transporting blood over long periods of time (Kamiya & Togawa 1980), whereas the flow may vary considerably within the physiological range. Therefore, it is of interest to examine the sensitivity to geometry over a range of flow conditions, in order to determine how well the design works. Finally, it is permissible to speculate whether an understanding of the influence of the three-dimensional geometry of arteries on the flow could have relevance beyond vascular function, for example in the design of general piping systems.

4. Endnote

The review by Berger *et al.* (1983) describes many of the results which have been obtained relating to flow in planar bends. It is found that the Dean number, which expresses the non-dimensional ratio of inertial and centrifugal forces to the viscous forces is a fundamental parameter. In theoretical studies, this is commonly given as $D = (Ga^2/\mu)(2a^3/R\nu^2)^{1/2}$, where a is the tube radius, R the radius of curvature, G the pressure gradient and μ, ν the dynamic and kinematic viscosities, respectively. A more useful form for comparison with measurements (which eliminates G), given by Berger *et al.* (1983), and referred to here as D_2, is $D_2 = (a/R)^{1/2}\, Re_{\mathrm{d}}$, where Re_{d} is the Reynolds number based on mean velocity and tube diameter. The quantities are related by $D = 2^{5/2}(Q_{\mathrm{s}}/Q_{\mathrm{c}})D_2$, and $Q_{\mathrm{s}}/Q_{\mathrm{c}}$ is the ratio of the flow rates in a straight to a curved pipe, which is calculated in the theoretical solution. $Q_{\mathrm{s}}/Q_{\mathrm{c}}$ is near unity at low D and rises to nearly 2.5 at $D = 5000$, (and there is a very weak additional dependence of $Q_{\mathrm{s}}/Q_{\mathrm{c}}$ on the form of the solution). Thus, $D < 1000$ in Dennis & Ng (1982) is equivalent to $D_2 < 114$, whereas $D = 2000$ corresponds to $D_2 \approx 191$. The Reynolds numbers and curvatures for the larger arteries are sufficient therefore to lie within the range in which Dennis & Ng (1982) found that either

two- or four-vortex secondary flow patterns could occur in steady planar curved pipe flow. In the work of Kao (1987) for a helical pipe, additional parameters $\epsilon = a\kappa$, and $\lambda = a\tau$ are involved in the analysis, where κ is the curvature and τ the torsion. Kao's (1987) results for $D = 2000$ show that for values of $\lambda = 0.16$ and $\epsilon = 0.05$, the secondary flow is considerably different from that of a planar curved tube, with one vortex producing a dominant rotation in one direction, and with asymmetry of the axial velocity contours.

L.Q. was a Royal Society Royal Fellow, People's Republic of China. We acknowledge help from Dr J. Mestel and Dr P. Cashman, Mr N. Watkins, and collaborations with Mr K. Robinson, and Professor B. Hillen, Drs J. Ravensbergen and J. Krijger, and Mr. P. Wensing, Utrecht University, The Netherlands. We thank St. Mary's NHS Trust for access to the MR scanner and BUPA Medical Foundation, BT Charity, 3M and HNE Healthcare for support.

References

Altobelli, S. A. & Nerem, R. M. 1985 An experimental study of coronary artery fluid mechanics. *Biomech. Engng* **107**, 16–23.

Asakura, T. & Karino, T. 1990 Flow patterns and spatial distribution of atherosclerotic lesions in human coronary arteries. *Circulat. Res.* **66**, 1045–1066.

Back, M. R., Cho, Y. I. & Back, L. H. 1985 Fluid dynamic study in a femoral artery branch casting of man with upstream main lumen curvature for steady flow. *J. Biomech. Engng* **107**, 240–248.

Batten, J. R. & Nerem, R. M. 1982 Model study of flow in curved and planar arterial bifurcations. *Cardio. Res.* **16**, 178–186.

Berger, S. A., Talbot, L. & Yao, L. S. 1983 Flow in curved pipes. *A. Rev. Fluid Mech.* **15**, 461–512.

Caro, C. G., Fitz-Gerald, J. M. & Schroter, R. C. 1971 Atheroma and arterial wall shear: observation, correlation and proposal of a shear dependent mass transfer mechanism for atherogenesis. *Proc. R. Soc. Lond.* B **177**, 109–159.

Caro, C. G., Dumoulin, C. L., Graham J. M. R. 1992 Secondary flow in the human common carotid artery imaged by MR angiography. *J. Biomech. Eng.* **114**, 147–149.

Caro, C. G., Doorly, D. J., Tarnawski, M., Scott, K. T., Johnson, M. J. & Dumoulin, C. L. 1994*a* Non-planar curvature and branching of arteries. *J. Physiol.* P **475**, 60P.

Caro, C. G., Tarnawski, M., Scott, K. T., Johnson, M. J., Doorly, D., Long, Q. & Dumoulin, C. L. 1994*b* Geometry and fluid mechanics of arterial curvature and branching. In *3rd Int. Symp. on Biofluid Mechanics* (Munich) suppl. 2-9. Dusseldorf: VDI.

Dennis, S. C. R. & Ng, M. C. 1982 Dual solution for steady laminar flow through a curved tube. *Q. Jl Mech. appl. Math.* **35**, 305–324.

Dobrin, P. B., Litooy, F. N. & Endean, E. D. 1989 Mechanical factors predisposing to intimal hyperplasia and medial thickening in autogenous vein grafts. *Surgery* **105**, 393–400.

Doorly, D. J., Tarnawski, M., Caro, C. G., Scott, K. T. & Cybulski, G. 1994 Unsteady arterial flow, distensibility and velocity distribution measurement techniques. *Clin. Haemorheol.* **14**, 426.

Dumoulin, C. L., Doorly, D. J. & Caro, C. G. 1993 Quantitative measurement of velocity at multiple positions using comb excitation and Fourier velocity encoding. *Magn. Reson. Med.* **29**, 44–52.

Farthing, S. & Peronneau, P. 1979 Flow in the thoracic aorta. *Cardio. Res.* **13**, 607–620.

Fox, B., James, K., Morgan, B. & Seed, W. A. 1982 Distribution of fatty and fibrous plaques in young human coronary arteries. *Atherosclerosis* **41**, 337–347.

Frangos, J. A., Eskin, S. G., McIntyre, L. V. & Ives, C. L. 1985 Flow effects on prostacyclin production by cultured endothelial cells. *Science* **227**, 1477–1479.

Frazin, L. J., Lanza, G., Vonesh, M., Khasho, F., Spitzzeri, C., McGee, S., Mehlman, F. D., Chandran, K. B., Talano, J. & McPherson, D. 1990 Functional chiral asymmetry in descending thoracic aorta. *Circulation* **82**, 1985–1994.

Friedman, M. H., Deters, O. J., Mark, F. F., Bargeron, C. B. & Hutchins, G. M. 1983 Arterial geometry affects hemodynamics: a potential risk factor for atherosclerosis. *Atherosclerosis* **46**, 225–231.

Germano, M. 1982 On the effect of torsion on a helical pipe flow. *J. Fluid Mech.* **125**, 1–8.

Henderson, A. H. 1991 Endothelium in control. *Br. Heart Jl* **65**, 116–125.

Hoydu, A. K., Bergey, P. D. & Haselgrove, J. C. 1994 A MRI bolus tagging method for observing helical flow in the descending *aorta. Magn. Reson. Med.* **32**, 794–800.

Johnson M. J., Caro, C. G., Scott, K. T., Doorly, D. J., Tarnawski, M. & Dumoulin, C. L. 1994 Indicator dispersion in planar and non-planar artery models. *J. Physiol.* P **475**, 11P.

Kamiya, A. & Togawa, T. 1980 Adaptive regulation of wall shear stress to flow change in the canine carotid artery. *Am. J. Physiol.* **239**, H14–H21.

Kao, H. C. 1987 Torsion effect on fully developed flow in a helical pipe. *J. Fluid Mech.* **184**, 335–356.

Karino, T., Takeuchi, S., Kobayashi, N. & Abe, H. 1994 Vascular geometry, flow patterns and preferred sites for aneurysm formation in human intracranial arteries. In *2nd World Cong. of Biomechanics* (Amsterdam) vol II, 259a.

Kilner, P. J., Yang, G. Z., Mohiaddin, R. H., Firmin, D. N. & Longmore, D. B. 1993 Helical and retrograde secondary flow patterns in the aortic arch studied by three-directional magnetic resonance velocity mapping. *Circulation* **88**, 2235–2247.

Liepsch, D. (ed.) 1990 *Biofluid mechanics: blood flow in large vessels. Proc. 2nd Int. Symp.* Berlin: Springer.

Liepsch, D. (ed.) 1994 *Biofluid mechanics: Proc. 3rd Int. Symp.* Dusseldorf: VDI.

Lou, Z. & Yang, W.-J. 1992 Biofluid dynamics at arterial bifurcations. *Crit. Rev. Biomed. Engng* **19**, 455–493.

Manlapaz, R. I. & Churchill, S. W. 1980 Fully developed laminar flow in a helically coiled tube of finite pitch. *Chem. Engng Commun.* **7**, 57–78.

Masawa, N., Glagov, S. & Zarins, C. K. 1994 Quantitative morphologic study of intimal thickening at the human carotid bifurcation: I. Axial and circumferential distribution of maximum intimal thickening in asymptomatic uncomplicated plaques. *Atherosclerosis* **107**, 137–146.

Moore, J. E., Maier, S. E., Ku, D. N. & Boesiger, P. 1994 Haemodynamics in the abdominal aorta: a comparison of *in vitro* and *in vivo* measurements. *J. appl. Physiol.* **76**, 1520–1527.

Mosora, F., Caro, C. G., Krause, E., Schmid-Schonbein, H., Baquey, C. & Pelissier, R. (eds) 1990 *Biomechanical transport processes.* New York: Plenum.

Ojha, M. 1994 Wall shear stress temporal gradient and anastomotic intimal hyperplasia. *Circulat. Res.* **74**, 1227–1231.

Pao, Y. C., Lu, J. T. & Ritman, E. L. 1992 Bending and twisting of an *in vivo* coronary artery at a bifurcation. *J. Biomech.* **25**, 287–295.

Perktold, K., Florian, H., Hilbert, D. & Peter, R. 1988 Wall shear stress distribution in the human carotid siphon during pulsatile flow. *J. Biomech.* **21**, 663–671.

Paulsen, P. K. & Hasenkam, J. M. 1983 Three-dimensional visualization of velocity profiles in the ascending aorta in dogs, measured with a hot-film anemometer. *J. Biomech.* **16**, 201–210.

Sabbah, H. N., Walburn, F. J. & Stein, P. D. 1984 Patterns of flow in the left coronary artery. *J. Biomech. Engng* **106**, 272–279.

Schettler, G., Nerem, R. M., Schmid-Schonbein, H., Morl, H. & Diehm, C. (eds) 1983 *Fluid dynamics as a localising factor for atherosclerosis.* Berlin: Springer.

Scholten, F. G. & Wensing, P. J. W. 1995 Atherogenesis in the distal part of the femoral artery: a functional anatomical study of local factors. Ph.D. thesis, University of Utrecht.

Secomb, T. W., Pries, A. R. & Gaehtgens, P. 1995 Architecture and hemodynamics of microvascular networks. In *Biological flows* (World Congress of Biomechanics Series 1) (ed. M. Jaffrin & C. G. Caro). New York: Plenum (in press).

Stonebridge, P. A. & Brophy, C. M. 1991 Spiral laminar flow in arteries? *Lancet* **338**, 1360–1361.

Stonebridge, P., Hoskins, P. & Allan, P. 1994 *In-vivo* stable spiral laminar flow. *Br. J. Surg.* **81**, 613.

Tompsett, D. H. 1967 Casts of the vessels of the head and vertebral column. *Br. J. Surg.* **54**, 719–723.

Wang, C. Y. 1981 On the low Reynolds-number flow in a helical pipe. *J. Fluid Mech.* **108**, 185–194.

White, S. S., Zarins, C. K., Giddens, D. P., Bassiouny, H., Loth, F., Jones, S. A. & Glagov, S. 1993 Hemodynamic patterns in two models of end-to-side vascular graft anastomoses. *J. Biomech. Engng* **115**, 104–111.

Yearwood, T. L. & Chandran, K. B. 1984 Physiological pulsatile flow experiments in a model of the human aortic arch. *J. Biomech.* **15**, 683–704.

Yoshida, Y., Yamaguchi, T., Caro, C. G., Glagov, S. & Nerem, R. M. (eds) 1988 *Role of blood flow in atherogenesis.* Tokyo: Springer.

Received 21 February 1995; revised 31 May 1995; accepted 31 July 1995